Surfaces, Interfaces, and Catalysis; Physical Properties of Nanomaterials and Materials

The Interface Structure in Li-Metal/[Pyr14][TFSI]-Ionic Liquid System from Ab Initio Molecular Dynamics Simulations

Boris V. Merinov, Sergey V. Zybin, Saber Naserifar, Sergey I Morozov, Julius Jacob Oppenheim, William A. Goddard, Jinuk Lee, Jae Hyun Lee, Hyea Eun Han, Young Cheol Choi, and Seung Ha Kim

J. Phys. Chem. Lett., **Just Accepted Manuscript** • DOI: 10.1021/acs.jpclett.9b01515 • Publication Date (Web): 25 Jul 2019

The Interface Structure in Li-Metal/[Pyr_{14}][TFSI]-Ionic Liquid System from Ab Initio Molecular Dynamics Simulations

Boris V. Merinov,*,† Sergey V. Zybin,† Saber Naserifar,† Sergey Morozov,‡ Julius Oppenheim,† William A. Goddard III,† Jinuk Lee,§ Jae Hyun Lee,§ Hyea Eun Han,§ Young Cheol Choi,§ and Seung Ha Kim§

†*Materials and Process Simulation Center (MSC), California Institute of Technology (Caltech), Pasadena, California, 91125, U.S.A.*

‡*South Ural State University, 76 Lenin Avenue, Chelyabinsk 454080, Russia*

§*Battery R & D, LG Chem, Yuseong-Gu, Daejeon 34122, Republic of Korea*

Abstract

Ionic liquids (ILs) are promising materials for application in a new generation of Li-batteries. They can be used as electrolyte, interlayer, or incorporated into other materials. ILs have ability to form a stable Solid Electrochemical Interface (SEI) which plays an important role, preventing Li-based electrode from oxidation and electrolyte from extensive decomposition. Experimentally, it is hardly possible to elicit fine details of the SEI structure. To remedy this situation, we have performed a comprehensive computational study (DFT-MD) to determine the composition and structure of the SEI compact layer formed between Li anode and [Pyr_{14}][TFSI] IL. We found that the [TFSI] anions quickly reacted with Li and decomposed, unlike the [Pyr_{14}] cations which remained stable. The obtained SEI compact layer structure is non-homogeneous and consists of the atomized S, N, O, F, and C anions oxidized by Li atoms.

TOC GRAPHIC ABSTRACT

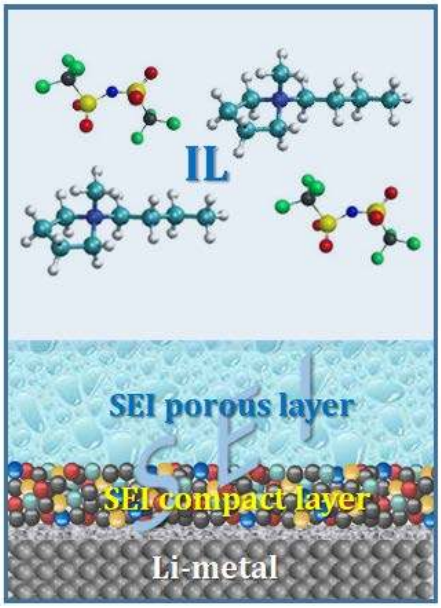

Today state-of-the-art Li-ion batteries have practically achieved their energy density limit, thus new strategies are needed for the dramatic improvements in performance and safety required for commercial applications.[1-7] Electrochemical systems based on solid electrolytes possess many advantages over liquid electrolyte-based devices (e.g. no electrolyte leakage, increased safety, higher energy density and stability, smaller size, faster charging, increased cycle life, greater flexibility with regard to battery placement and vehicle design) and have potential to overcome the disadvantages of the liquid electrolyte battery technology. These systems could be even more efficient and provide the highest energy densities if used in combination with Li-metal anode. Unfortunately, Li-metal is highly reactive and typically decomposes the solid electrolyte if in contact and the products formed generally have a significantly lower ion-conductivity than that of the solid electrolyte. This results in growth of a resistive layer during charge/discharge cyclings which leads to degradation of the interfacial properties and deterioration of battery performance.

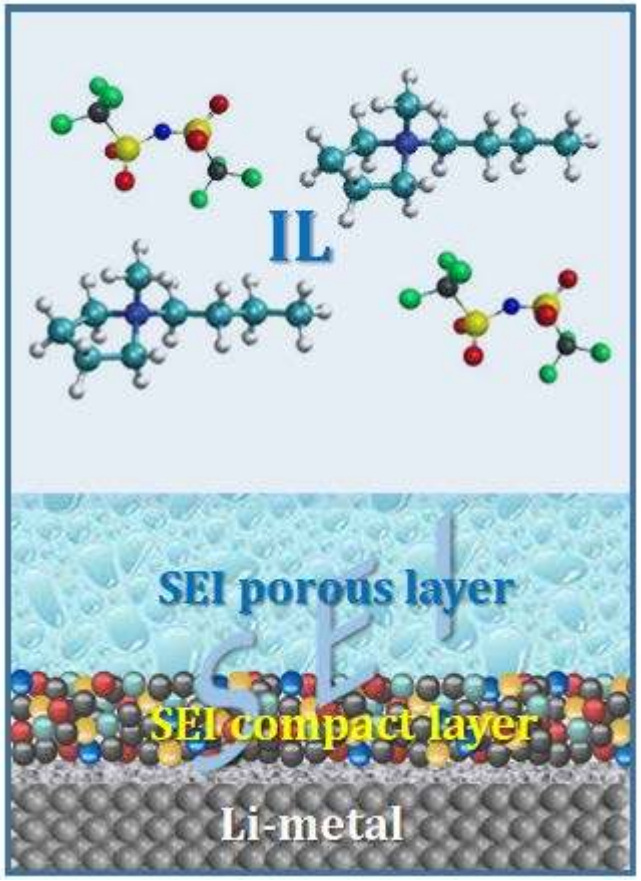

Figure 1. Schematic representation of the interface between a lithium anode (Li-metal) and ionic liquid (IL).

Ionic liquids (ILs) have attracted attention of researchers as suitable candidates for battery applications since the late 1990's.[8-10] They exhibit a number of advantages such as negligible volatility, relatively high decomposition temperatures, suitable ionic conductivity (up to ~10^{-4} S/cm), and wide electrochemical windows.[11-14] ILs can be used as electrolyte, interlayer, or incorporated into other materials. They are also known their ability to form a stable Solid Electrolyte Interface (SEI) on lithium and graphite anodes.[15,16] This SEI is observed on the lithium surface and plays an important role in Li-ion batteries, preventing the Li-based electrode from comprehensive oxidation and the electrolyte from extensive decomposition. The SEI structure and composition varies and depends on the electrolyte and electrode materials. Generally, SEI is considered as consisting of two layers, compact (inorganic solid phase) and porous (organic-containing phase).[17-22] The compact layer forms close to the electrode surface and is assumed to be ~10 Å thick.[17] The porous layer grows ontop of the compact layer and has a higher Li-ion diffusion coefficient than that of the compact layer, but lower electronic conductivity.[18] It will stop growing when electrolyte can no longer receive electrons from the electrode and, therefore, it cannot be further reduced. In Li-ion batteries with conventional liquid electrolyte, the electrolyte degradation occurs during both charge-discharge cyclings and storage. The interfacial resistance of fresh lithium with traditional liquid electrolyte, is relatively small. However, it increases

continuously during storage and becomes 10 times higher after 10 days of storage.[23] The interfacial resistance continues increasing but slower during further storage. This means that the SEI formed on the lithium surface is unstable even without any electrochemical reactions and it takes long time to form a relatively stable SEI. In contrast, a thick passivation SEI forms immediately on the lithium surface, when the 4[Pyr_{14}][TFSI] IL is used as electrolyte, and this SEI is relatively stable over repeated cycles.[23]

However, only limited information is available about the SEI composition and structure, providing very little guidance for choosing ILs that would lead to the best SEI performance. Experimentally, it has not yet been possible to elicit fine details of the SEI structure. To remedy this situation, we have performed a computational study to determine the composition, structure, and properties of the SEI formed between the lithium anode and specific ILs (Figure 1).

Among ILs, *N*-butyl-*N*-methylpyrrolidinium (Pyr_{14}^+) with bis(trifluoromethanesulfonyl)imide ($TFSI^-$) doped with [Li][TFSI] salt is considered as a good candidate for battery applications.[24-26] Earlier, this system was studied by Yildirim and Haskins et al.[27,28] using a maximum of 40 ps of DFT based Molecular Dynamics (DFT-MD, also called *Ab Initio* MD) to determine decomposition reactions and products at the Li/IL interface. Their simulations revealed spontaneous [TFSI] decomposition, while no decomposition was noted for [Pyr_{14}]. However, the authors of this work did not pursue a fully equilibrated atomistic structure of the Li/IL interface.

In our article, we focus on the structural aspects of the SEI, in particular, on the compact layer of the SEI which may cause rate limitations in Li-ion batteries.[29] We anticipate that determining the structure and resulting materials properties may provide the information useful for optimizing the SEI. This is the first study reporting a detailed atomistic description of the SEI structure formed at the interface of Li with an IL. The SEI structure was obtained from the DFT-MD simulations of the Li/[Pyr_{14}][TFSI] system. During this system equilibration, we found that the [Pyr_{14}] cations remained stable and moved away from the Li surface, while the [TFSI] anions strongly interacted with it and quickly decomposed. This differs dramatically from the [TFSI] anions, which quickly reacted with Li and decomposed. Similar results were obtained in ref. 27. This observation is consistent with experimental results which indicate that the main contribution to the SEI-film formed on the Li-anode, when [Pyr_{14}][TFSI] IL doped with [Li][TFSI] is used as electrolyte, comes from the decomposition of the [TFSI] anion.[30] The corresponding Pyr_{14} cations are possibly embedded in the reduction products of [TFSI] anions, such as LiF, Li_2O, Li_2S, NSO_2, etc., in the SEI porous layer and balanced by $(SO_2CF_3)^-$ or unreacted [TFSI] anions.[23,31]

Taking into account the weak interaction of the [Pyr_{14}] cations with the Li surface, we exchanged them with Li atoms to make a smaller model suitable for long DFT-MD simulations. Two systems, a smaller with 83 Li and 2 [TFSI] and larger with 164 Li and 4 [TFSI], were built and studied. The smaller system made it practical to run a much longer simulation, 723 ps *vs.* 164 ps for the larger system. Note that the Li-metal part in our simulations should rather be considered as amorphous Li than crystalline. The calculated Li–Li pair radial distribution function (RDF) (Figure S1 in Supporting Information) has a first peak at ~2.8 Å which is a typical value for the Li–Li distance in amorphous Li,[32,33] which is shorter than that in the crystalline Li-metal structure (3.02 Å).[34]

Reactive DFT-MD on the smaller 83Li/2[TFSI] system. First, we will analyze the evolution of the smaller 83Li/2[TFSI] system and formation of the SEI during the 723 ps NVT DFT-MD at 400 K (Figure S2 in Supporting Information). Both [TFSI] were completely atomized and oxidized by the Li surface after 450 ps of the DFT-MD simulation.

Initially, one of the N-S bonds in the [TFSI] broke forming two fragments, SO_2–CF_3 and N–SO_2–CF_3 (Figure 2). The fragment without the N atom quickly decomposed (during less than 10 ps), first, breaking three C–F bonds, then two S–O bonds, and finally the C-S bonds. The fragment with the N atom needed much longer time (about 450 ps) to completely decompose to full anion atomization. The step sequence of this decomposition was similar to that for the fragment without N, except for the S–N bond dissociation at the end.

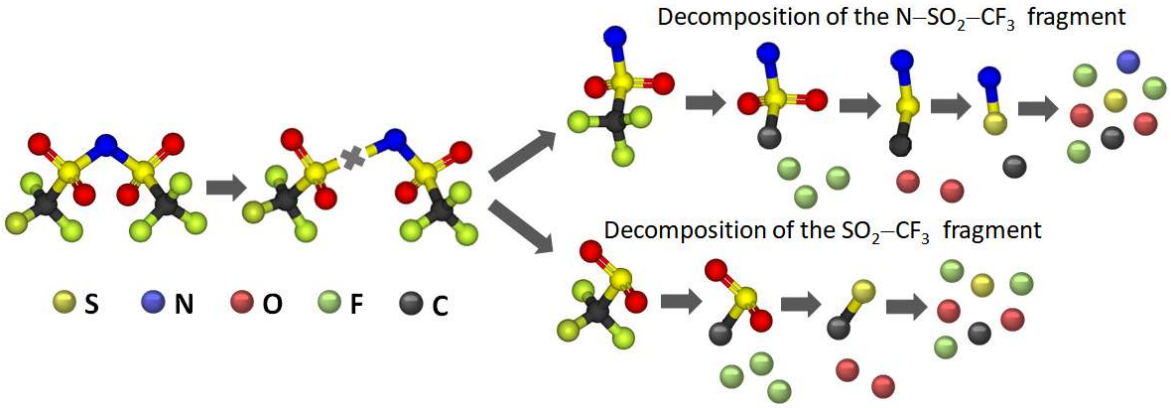

Figure 2. The [TFSI] decomposition sequence in the 83Li/2[TFSI] system. The SO_2–CF_3 fragment quickly decomposed (during less than 10 ps), while the complete decomposition of the N–SO_2–CF_3 fragment required about 450 ps.

To understand the SEI structure, we calculated relative element concentration distributions along the z-direction for the final frame of our DFT-MD simulation on the 83Li/2[TFSI] periodic system (Figure 3a). It is clearly seen that the SEI compact layer is non-homogeneous. The N and C atoms are closest to the Li surface, while the F atoms are spread through the remaining part of the compact layer with a trend for the relative concentration of these atoms to be higher closer to the edge of the compact layer. As for the S atoms, they occupy positions both in the middle and close to the edge of the compact layer.

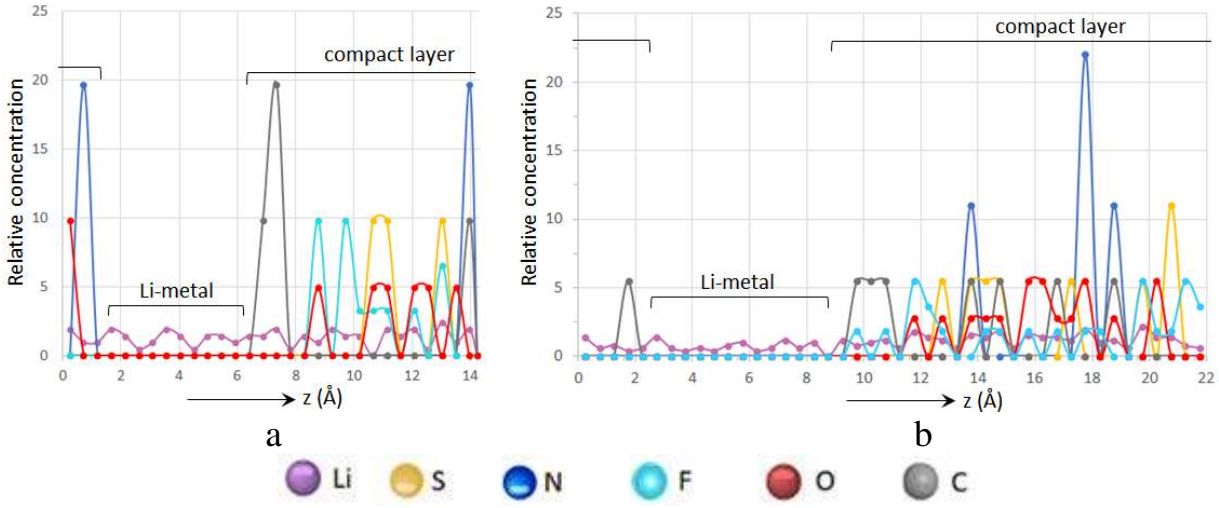

Figure 3. Relative element concentration distributions along the z-direction in the (a) smaller 83Li/2[TFSI] and (b) larger periodic 164Li/4[TFSI] systems.

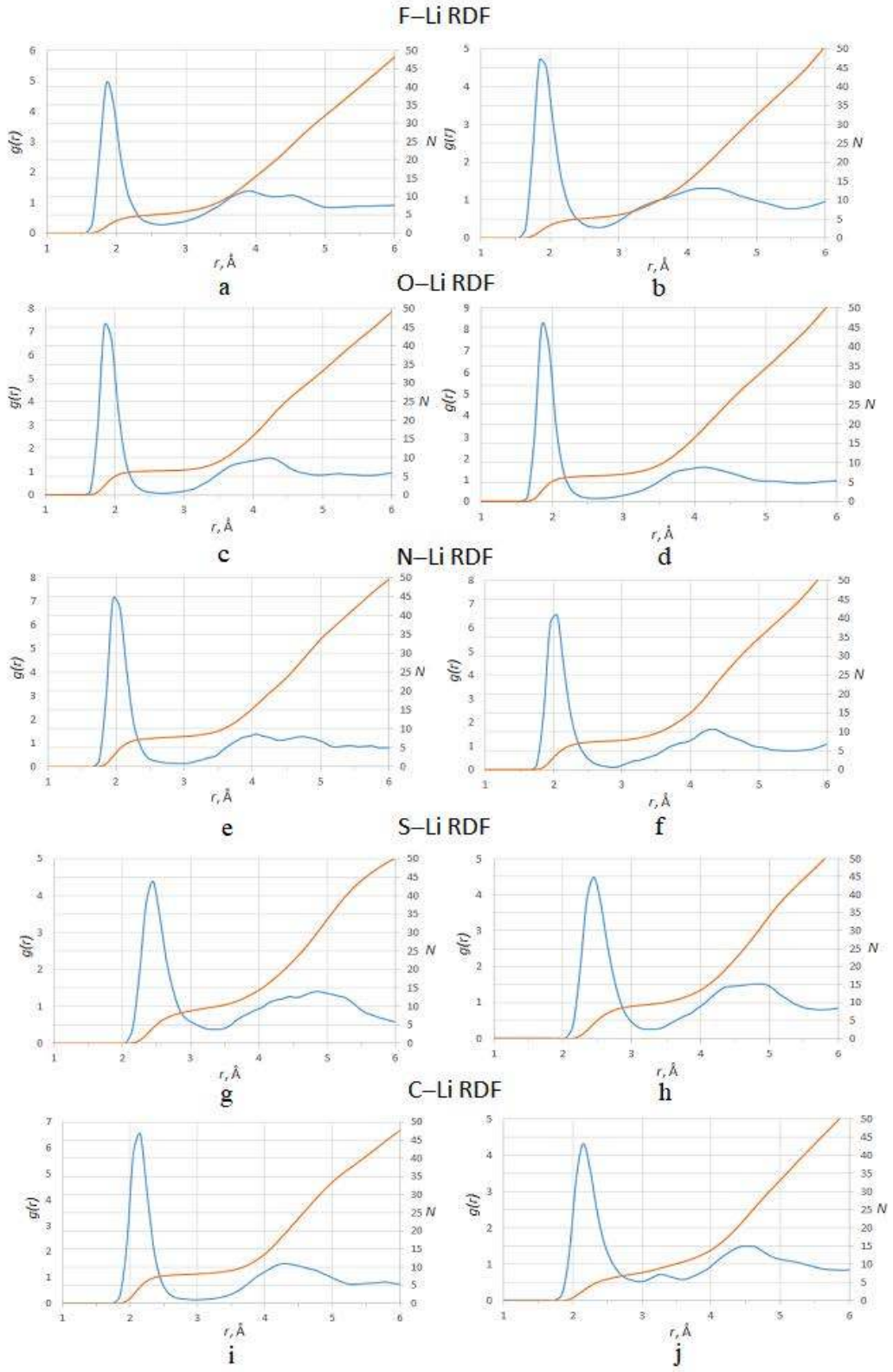

Figure 4. Pair RDFs (*g(r)*, blue, left axis) and integrated number of bonds (*N*, orange, right axis) for the smaller 83Li/2[TFSI] (right) and larger 164Li/4[TFSI] (left) systems.

To better describe the SEI, we calculated and analyzed RDFs, *g(r)*, for all Li–X (X=N, S, O, and C) pairs and the integrating *g(r)* to find the average coordination number (*N*) of each type of bonds (Figure 4). Then we examined the actual structure to determine atomic environments around the F, O, N, S and C anions. We used the last frame of our simulation to show examples of these environments (Figure 5).

The F atoms in the SEI form bonds only with Li atoms. The F–Li RDF has a first peak at ~1.8 Å (Figure 4a), corresponding to F–Li bonds. The typical coordination number for the F atoms is 4 or 3 (Figure 5a, b). The length of the F-Li bonds varies from 1.7 to 2.0 Å. No other F-X bonds are observed at the end of our simulation (Figure S3 in Supporting Information). This Li_nF formation is consistently found as a main SEI components in conventional Li-ion batteries and plays an important role in the morphological and compositional picture of the SEI.[29]

Next, we consider bonds and atomic environments around O atoms. Similar to the F atoms, the O atoms in the SEI are bonded only with Li atoms. The O–Li RDF with the first peak at ~1.8 Å corresponding to the O–Li bonds is shown in Figure 4c. The O atoms in the SEI are mostly coordinated with five or six Li atoms (Figure 5c) and sometimes with four Li atoms (Figure 5d). The typical O–Li bond length is 1.9–2.0 Å.

There are two N atoms in our smaller SEI compact layer structure. The N–Li RDF with a peak at ~2.0 Å is shown in Figure 4e, and atomic environments in which N atoms are directly bonded to Li atoms can be viewed in Figure 5e, f. The first N atom forms four N–Li bonds. The length of these bonds varies from 1.69 to 2.01 Å. The second N atom is coordinated with three Li atoms. The corresponding bond lengths are 1.78, 1.80, and 1.81 Å. From the N–Li RDF, we can say that the N atoms may have up to six Li neighbors within 2.2 Å.

The S–Li RDF has a first peak at ~2.3 Å (Figure 4g), a normal S–Li bond length. The number of Li neighbors for the S atoms varies from 1 to 3: two S atoms have three Li neighbors (Figure 5g, h), and two remaining S atoms are coordinated with two and one Li atoms, respectively (Figure 5i, j). The length of the S–Li bonds lies in the range of 2.20 to 2.35 Å. One of the S atoms, coordinated with three Li atoms, has an additional bond of 1.89 Å with a C atom (Figure 5g). The S–Li RDF shows that the S atoms may have up to 5 Li neighbors within 2.5 Å.

All S-F, S-O, and S-N, distances are over 3 Å (Figure S3 in Supporting Information) and, therefore, the above bonds are not observed in our simulation.

As for the C atoms, the corresponding C-Li RDF has a peak at ~2.1 Å (Figure 4i) and all of them are coordinated with two Li atoms (Figure 5k-n). As it was mentioned above, one of them has the additional bond with the S atom (Figure 5n). The C-Li distances varies from 1.9 to 2.1 Å. The C-Li RDF shows that the C atoms may have up to 7 Li neighbors within 2.5 Å.

DFT-MD on the larger system and comparison to the smaller. In addition to the smaller Li/TFSI system of 113 atoms, we carried out DFT-MD simulations on the larger system with 224 atoms for 164 ps. We calculated a relative element concentration distribution for the Li atoms at 12, 22, 32, 42 and 52 ps (Figure S4 in Supporting Information). Analyzing this distribution, we find that after 12, 22, and 32 ps DFT-MD, additional 2, 18 and 24 Li, respectively, from the Li-metal part moved to the SEI and reacted with the SEI anions. However, after 42 and 52 ps, 8 and 9 Li atoms, respectively, moved back from the SEI to the Li metal part. This indicates that the system is fully equilibrated as for Li and can be used for further calculations of the system properties, for instance, diffusion constants.

Comparing the concentrations along the z-direction for the final frames of the DFT-MD simulations on the smaller and larger systems (Figure 3a, b), we see that both systems consist of a

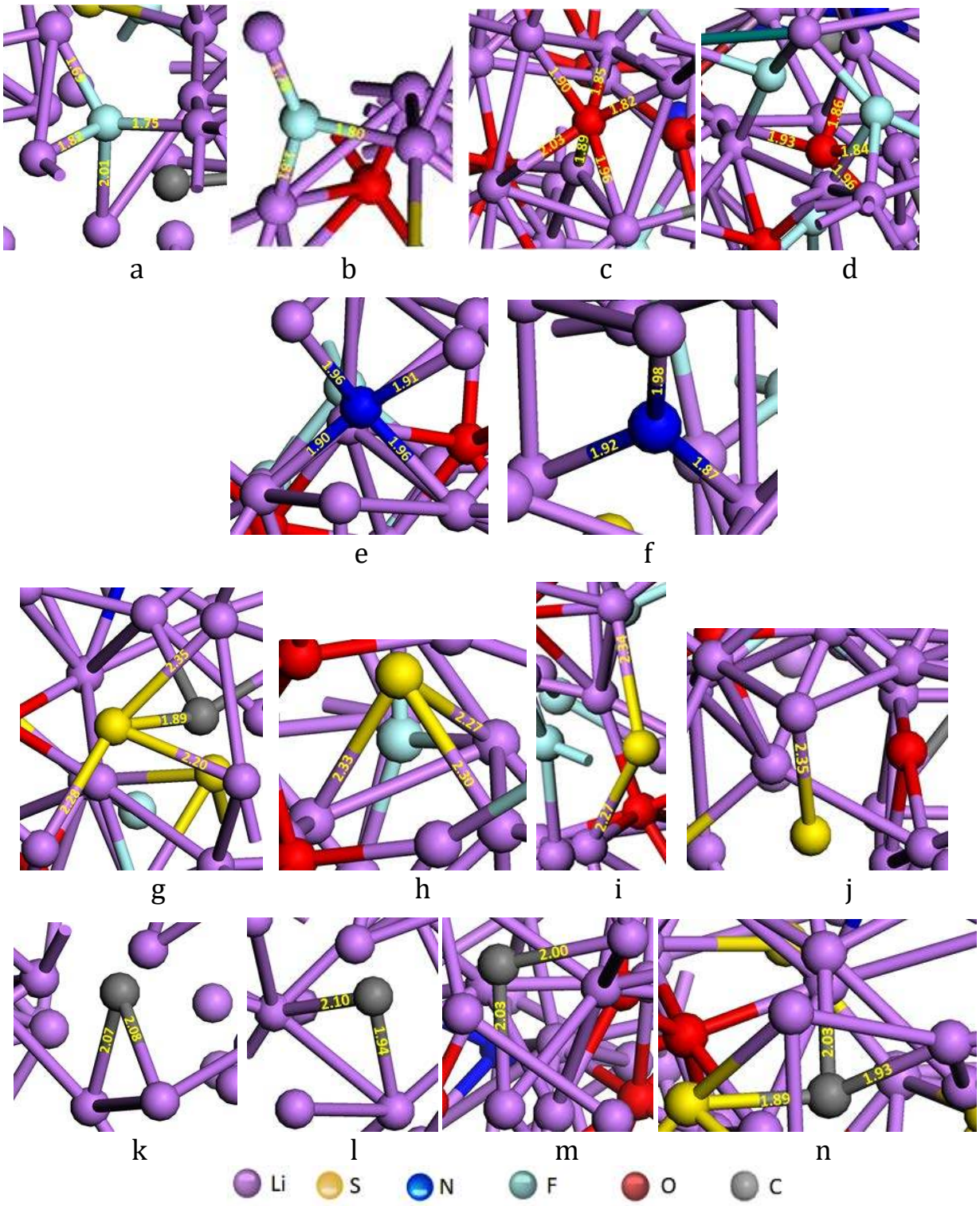

Figure 5. Examples of the anion environments in the SEI: (a, b) 4- and 3-coordinated F atoms coordinated with 4 and 3 Li atoms, (c, d) O atoms coordinated with 6 and 4 Li atoms, (e, f) N atoms coordinated with 4 and 3 Li atoms, (g) S atom coordinated with 3 Li and 1 C atoms, (h, i, and j) S atoms coordinated with 3, 2 and 1 Li atoms, respectively, (k, l, m) C atoms coordinated with 2 Li atoms, and (n) C atom coordinated with 2 Li and 1 S atoms.

Li metal region coupled an SEI compact layer. The Li atoms are evenly distributed through the whole systems while the O atoms are evenly distributed over the full SEI compact layer.

In the smaller system, the F atoms are generally in the SEI compact layer core with a trend for the relative concentration of these atoms to be higher closer to the edge. In the larger system, this trend is more pronounced and the F concentration is clearly higher closer to the edges of the compact layer than in the core. (Figure 3).

The environments around F and O atoms in both systems are very similar. The related RDFs (Figures 4a, b and c, d) are almost identical. In both systems, the typical coordination number of oxygen varies from 4 to 6, but mostly 6, while that of fluorine is 3 or 4.

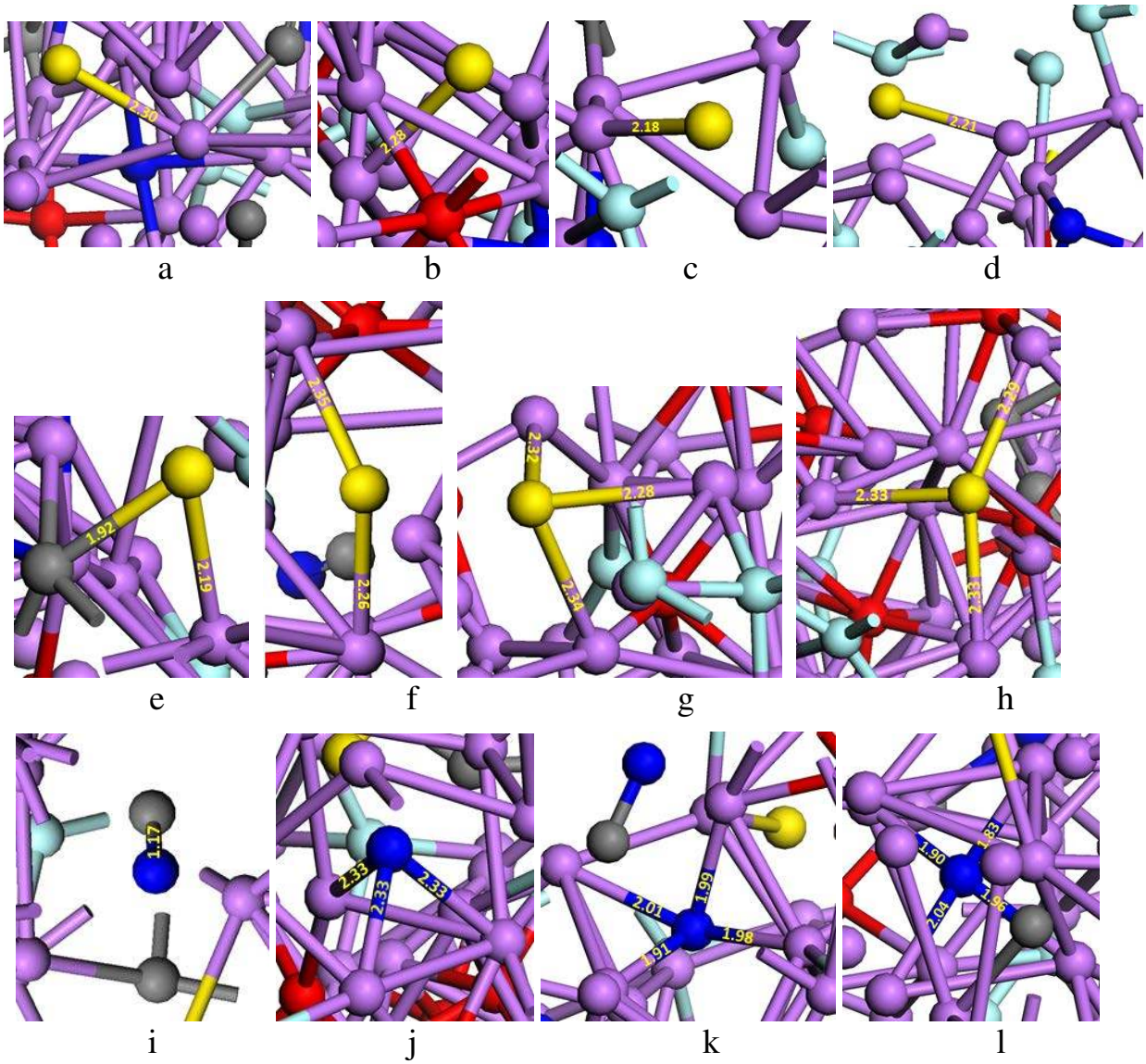

Figure 6. The environments of the S (a-h) and N (i-l) atoms in the SEI of the larger Li/TFSI system.

In the larger system, the S atoms are mostly in the SEI compact layer core (six of the eight S atoms) with two S atoms closer to the edge, while half of the four S atoms are in the core and half closer to the edge in the smaller system (Figure 3).

The S-Li RDFs are very similar for both systems (Figure 4g, h). Five of the eight S atoms in the larger system are coordinated with only one Li atom (Figure 6a-e) at 2.18 to 2.30 Å, and one of them has an additional bond with a C atom with a length of 1.92 Å (Figure 6e). Three remaining S atoms are coordinated with two or three Li atoms at 2.26 to 2.33 Å (Figure 6f-h).

Unlike the smaller Li/TFSI system, where the N atoms occupy positions at the edge of the SEI compact layer, all four N atoms in the larger Li/TFSI system are in the SEI compact layer core (Figure 3). The N–Li RDFs for the smaller and larger systems are very similar, both have the first peak at 2.0 Å (Figures 4e, f). One of the N atoms is bonded with a C atom forming a C–N cyano group with an interatomic distance of 1.17 Å (Figure 6i). We do not find a C–N group in the smaller Li/TFSI system. The other N atoms are coordinated with 3 or 4 Li atoms at distances of 1.83 to 2.33 Å (Figure 6j-l). The 2.33 Å is related to the 3-coordinated N atom. The N–Li distances for the 4-coordinated N atoms are shorter and vary from 1.83 to 2.04 Å. Similar 3- and 4-coordinations are observed in the smaller system.

The main difference between the SEI in the larger and smaller Li/TFSI systems was found for the C atom environments. In addition to the C–N group, two C_2 molecules are observed only in the larger system. The corresponding peak at 1.3 Å is detected in the C–C RDF (Figure 7a). In both C_2 molecules, one of the C atoms has two Li neighbors, while the other one is bonded only

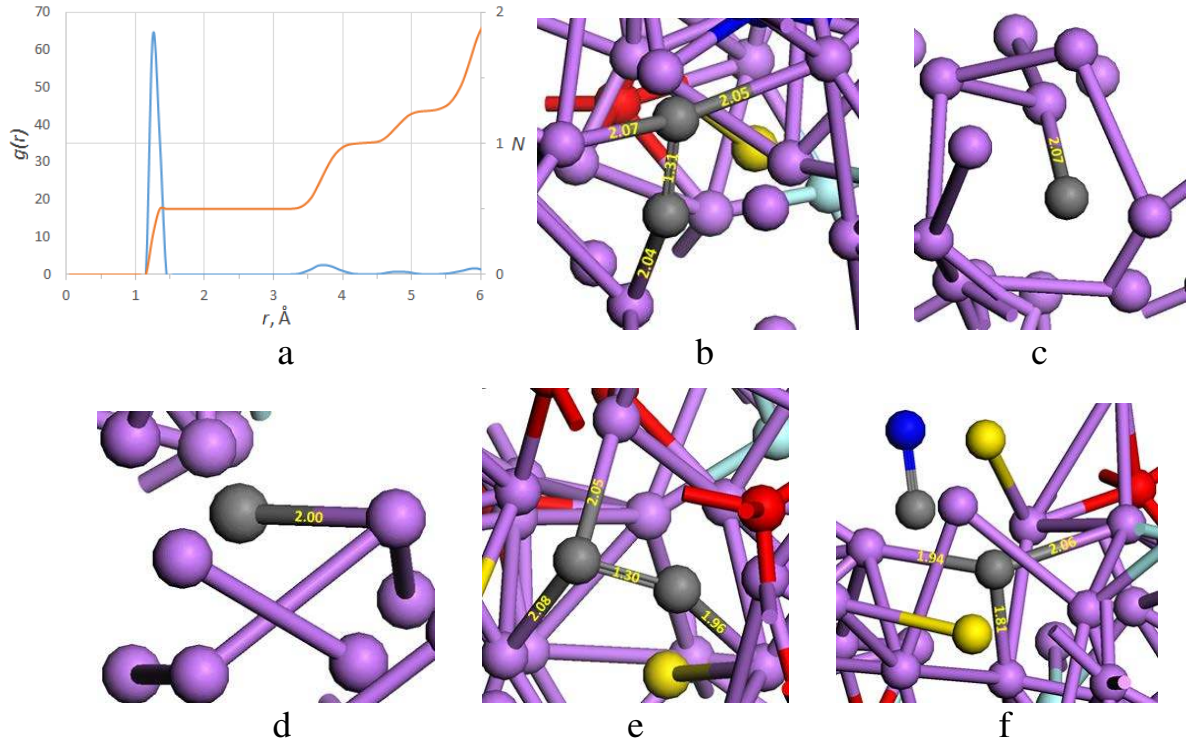

Figure 7. (a) The C–C RDF for the larger 164Li/4[TFSI] system; (b) one C_2 molecule and (c, d) two Li atoms at the edge of the SEI compact layer ; (e) one C_2 molecule, (f) one Li atom and C–N in the SEI core.

with one Li atom (Figure 7b, e). Most of the related C–Li distances are close to each other, from 2.04 to 2.08 Å. Only one of the distances is slightly shorter, 1.96 Å.

Two of the three remaining C atoms form bonds only with one Li atom with the corresponding length of 2.00 and 2.07 Å, and the last C atom has 3 Li neighbors at 1.81, 1.94 and 2.06 Å. In the smaller system, the C atoms are bound only to one or two Li atoms. The C–Li RDFs are very similar for the smaller and larger systems and have the first peak at ~2.1 Å (Figure 4i, j).

The C atoms are evenly distributed through the SEI compact layer, unlike the smaller system, where all C atoms were found at the compact layer edge (Figure 3). One of the C_2 molecules and two C atoms are at the edge (Figure 7b-d), while the other C_2 molecule along with C–N and one C atom occupy positions in the SEI compact layer core (Figure 7e, f). We consider this retention of C_2 bonds for the larger system is because the simulation time is only 164 ps. For the smaller system it required 450 ps to fully atomize the system.

The vibrational spectrum of the Li/TFSI systems. For further description of the systems, we calculated the vibrational density of states, DoS(ν), for all atoms together and for each sort of atoms in the smaller (Figure 8a) and larger (Figure 8b, c) Li/TFSI systems at 400 K and 1 atm. The power spectrum was determined using the 2PT methodology.[35-39] In this methodology, the DoS(ν) is computed from the Fourier transform of the velocity autocorrelation function. The broad peaks from 0 to 1000 cm^{-1} indicate interatomic modes of particles, which can be described as hindered translational modes. The higher frequency modes (>1000 cm^{-1}) correspond to intramolecular vibrations. The inset of Figure 8a provides a closer view and shows that there is no additional peak at larger frequencies (> 1000 cm^{-1}) for the smaller system (83Li/2[TFSI]). However, for the larger system (164Li/4[TFSI]), there is clearly a peak around 1800-1900 cm^{-1} (see the inset of Figure 8b). This peak is associated with formation of C_2 which is agreement with experimental data.[40] In Figure 8c, we further analyze the nature of the second peak by computing the DoS(ν) for C-N interactions. To do this, we first calculate the DoS(ν) for a group containing all of C and N atoms and then subtract from it the DoS(ν) for C and the DoS(ν) for N atoms. The results show that comparing to the total DoS(ν), there is a negligible formation of C-N and N_2 and

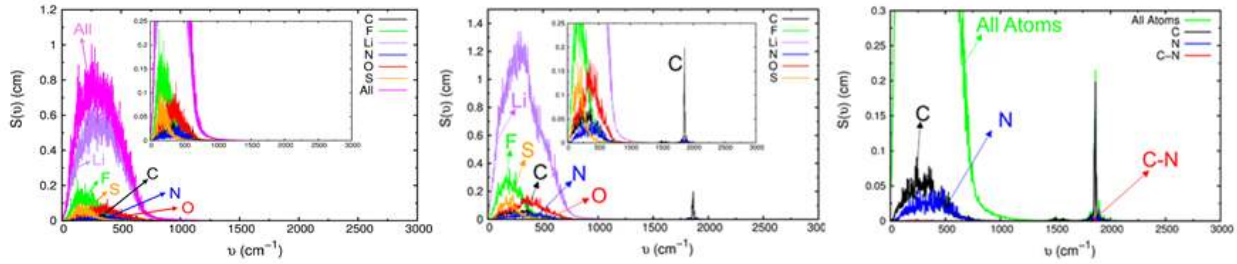

Figure 8. (a) Vibrational density of state functions, DoS(ν), for the smaller 83Li/2[TFSI] system at 400 K and 1 atm during the 673 to 723 ps time interval. The broad first peak shows the translation mode of each species in the system. There is not any peak for larger vibrational frequency. (b, c) DoS(ν) for the larger 164Li/4[TFSI] system at 400 K and 1 atm during the 144 to 164 ps time interval (b) for each sort atom separately and (c) for all atoms together and for C, N, and C-N. The broad first peak in (b) shows the hindered translation intermolecular modes for each species. The negligible peaks of C-N and N around 1800-1900 cm^{-1} in (c) show that the second peak is mainly associated with the C-C intramolecular interaction.

therefore the second peak is predominately due to C_2 formation in the larger system. We think that these modes would disappear, if the DFT-MD for the larger system would be extended over 450 ps.

In conclusion, we predicted the atomistic structure of the SEI for Li and [Pyr_{14}][TFSI] ionic liquid at 400 K, using DFT-MD. Two systems were studied: 83Li/2[TFSI] (113 atoms) and 164Li/4[TFSI] (224 atoms), for simulation times of 723 ps and 164 ps, respectively. The thickness of the obtained SEI compact layer in both systems is ~10 Å, which is in good agreement with the earlier made estimation.[17]

In the smaller system, the TFSI anions were completely decomposed during the first 450 ps of the 723 ps DFT-MD, with all F, S, O, N, and C anions atomized and oxidized by Li atoms. Here all C atoms occupy positions at the edges of the SEI compact layer. The distribution of the elements in the SEI compact layer is non-homogeneous. Some of them, such as Li and O, are almost evenly spread through the SEI compact layer, while the others, such as C and N, occupy positions at the edge of the SEI compact layer close to the Li-metal.

The main difference between the SEIs in the larger and smaller Li/TFSI systems was found for the C atom environments. Two C_2 molecules and one C–N group were observed only in the larger system. We think that this difference might be attributed to the insufficient simulation time of 164 ps for the larger system and would disappear at the simulation time over 450 ps.

To design the SEI with improved characteristics, it is required to determine the structure-property relationships. However, direct probes of the SEI structure and properties using experimental techniques are hardly possible, because of the thinness of the SEI and presence of other components of the system. Thus, the SEI structure-property relationships still remains largely unknown. The results on the SEI structure in the Li/IL system, reported in our paper, gives an opportunity to start identifying these relationships at the atomistic level.

Full DFT-MD on such systems for over 700 ps is an enormously long calculation, far too expensive for routine studies. The important lesson is that with sufficient Li available and sufficient time, the TFSI was fully decomposed with only Li in the first coordination even for C. Such calculations are far too expensive for full simulation of the charging and discharging of a battery where we need a realistic concentration of Li in the ionic liquid with examination of electric field driven diffusion. For such studies we need to develop a Reactive force field, such as ReaxFF.[41] Our DFT-MD calculations now set the stage for detailed training of the reactive FF needed for MD simulations on larger Li/IL models closer to realistic systems. We have now initiated these developments.

Computational methods and model building. To determine the dynamics of formation and properties of the SEI at equilibrium density, we performed DFT-MD simulations using the Vienna Ab Initio Simulation Package (VASP)[42-44] which implements the projector augmented wave (PAW) method for DFT. For all DFT-MD simulations, we use the Perdew-Burke-Ernzerhof generalized gradient approximation (GGA-PBE)[45] with the D3 (Becke-Johnson) empirical corrections[46,47] for long-range pairwise van der Waals attractive forces (approximating the London dispersion). This PBE-D3 level of DFT has been validated for several molecular systems, including DFT-MD simulations of metal-organics and Li-ion battery interfaces in particular.[27,28,48-50]

The energy cutoff for the plane-wave basis expansion was chosen at 500 eV, which was verified to provide converged forces by a test calculation at 600 eV. For the bulk Brillouin zone integration, a Γ-centered k-point mesh was used in all DFT-MD simulations within the supercell. A conjugate gradient algorithm was employed to relax the ion positions to obtain initial optimized structures. The initial velocities of the DFT-MD were chosen from the Maxwell-Boltzmann distribution with

a temperature of 20 K. The temperature during DFT-MD was maintained using a Nose-Hoover thermostat. We increased the temperature from 20 to 400 K within 1 ps, and then kept the temperature constant at 400 K in all our DFT-MD simulations. According to experimental results,[24] the higher the temperature, the faster SEI formation in Li/[Pyr_{14}][TFSI]/Li cells. The DFT–MD computation is extremely resource-demanding and the increased temperature, 400 K, is selected in order to accelerate the chemical reactions leading to the SEI formation, which enabled to decrease the time of our simulations.

The temperature fluctuations were within the interval of 350–450 K, with an RMS deviation of ~50 K. The integration time step was 1 fs.

The VASP code outputs the time evolution of the total energy of electrons and ions without kinetic energy of ions E(t), kinetic energy of ions $E^{ikin}(t)$, virial contribution to the pressure from the forces on electrons and ions $p^{ext}(t)$, and the kinetic pressure contribution of ions $p_i^{kin}(t)$ estimated from the ideal gas correction. At the equilibrium state of the simulated systems, its thermodynamic properties are obtained by averaging over the time with corresponding estimate of the statistical RMS errors.

In order to determine the equilibrium SEI structure for the Li/IL interface, we started with a system containing five layers of the Li(100) surface, each with 16 Li atoms, and four units of [Pyr_{14}][TFSI] in a cell box with $a = b = 13.7595$ and $c = 22.0000$ Å (Figure S5a in Supporting Information). Using DFT-MD, we optimized this system, heated it to 400 K, and equilibrated at 400 K for ~30 ps using the NVT ensemble. During this equilibration, the [Pyr_{14}] cations remained stable and moved away from the Li surface, whereas the [TFSI] anions reacted with the Li surface and decomposed. Since the [Pyr_{14}] cations did not participate in the SEI formation, we exchanged them with Li atoms. The vacuum, formed after the extraction of the [Pyr_{14}] from the system, was removed so that the final Li/4[TFSI] system used consisted of 84 Li atoms and 4 [TFSI] anions, totaling 144 atoms, with a cell box of $a = b = 12.3465$ and $c = 11.5127$ Å. As the reactions of [TFSI] with Li proceeded, the density increased due to formation of new bonds leading to a significantly decrease in the total pressure. To keep the equilibrium state with pressure of ~0 GPa, the c parameter of the cell dimensions was continuously readjusted as the calculations proceeded.

After 150 ps DFT-MD simulation on the 84Li/4[TFSI] system at 400 K, we found that two [TFSI] anions were completely decomposed and the corresponding F, O, N, and S atoms were oxidized with Li atoms, while the two remaining [TFSI] were only partially decomposed with such fragments as N–S–C and N–S that did not react further. We assumed that probably 80 Li atoms might be insufficient to complete decomposition reactions of 4 [Li][TFSI]. So, 5 additional layers of Li (80 atoms) were added (Figure S5b in Supporting Information) and the DFT-MD method was continued for another 164 ps to obtain a fully reacted [Li][TFSI] next to the Li electrode. This included 8 C, 24 F, 4 N, 16 O, 8 S, and 164 Li atoms, totaling 224 atoms with a Li:TFSI ratio of 41:1, with a cell box of $a = b = 11.5542$ and $c = 22.4420$ Å.

We also built a second Li/TFSI system with 81 Li atoms and 2 [Li][TFSI] molecules, 113 atoms totally (Figure S5c in Supporting Information), leading to a similar Li:TFSI ratio of circa 41:1. After readjustment and optimization of this system, the cell box dimensions, corresponding to approximately 0 GPa pressure, were $a = b = 10.080$ and $c = 14.200$ Å.

We used the 2PT methodology[35-39] to calculate the vibrational density of the states, DoS(ν), for all atoms. The 2PT methodology obtains accurate entropy and free energy information from short (~20 ps) dynamics, allowing for analysis during reactions and phase transitions. The 2PT approach uses the Fourier transform of the velocity autocorrelation function to obtain the power spectrum DoS(υ) which is corrected for diffusional contributions and then used to calculate the

thermodynamic properties by applying quantum statistics. We use 2PT to predict thermodynamic properties across interfaces.

Supporting Information

Evolution of the interface structure during the simulations; pair radial distribution functions (RDFs); relative Li concentration along the z-direction; the initial system models.

Acknowledgement

This work was supported by a research grant from LG Chem. S.M. is thankful for the support by Act 211 Government of the Russian Federation, under No. 02.A03.21.0011 and by the Supercomputer Simulation Laboratory of the South Ural State University.[51]

References

1. Thackeray, M. M.; Wolverton, C.; Isaacs, E.D. Electrical Energy Storage for Transportation—Approaching the Limits of, and Going Beyond, Lithium-ion Batteries. *Energy Environ. Sci.* **2012**, *5*, 7854-7863.
2. Evarts, E.C. To the Limits of Lithium. *Nature* **2015**, *526*, S93-S95.
3. Jiang, F.; Peng, P. Elucidating the Performance Limitations of Lithium-ion Batteries due to Species and Charge Transport through Five Characteristic Parameters. *Sci. Rep.* **2016**, *6*, 32639.
4. Blomgren, G. E. The Development and Future of Lithium Ion Batteries. *J. Electrochem. Soc.* **2017**, *164*, A5019-A5025.
5. Sripad, S.; Viswanathanz, V. Evaluation of Current, Future, and Beyond Li-Ion Batteries for the Electrification of Light Commercial Vehicles: Challenges and Opportunities. *J. Electrochem. Soc.* **2017**, *164*, E3635-E3646.
6. Hart, D.M. Making "Beyond Lithium" a Reality: Fostering Innovation in Long-Duration Grid Storage. ITIF, November 2018, 1-31.
7. Sripad, S.; Viswanathan, V. Performance Metrics Required of Next Generation Batteries to Make a Practical Electric Semi Truck. *ACS Energy Lett.* **2017**, *2*, 1669−1673.
8. Bonhote, P.; Dias, A.-P.; Papageorgiou, N.; Kalyanasundaram, K.; Gratzel. M. Hydrophobic, Highly Conductive Ambient-Temperature Molten Salts. *Inorg. Chem.* **1996**, *35*, 1168 –1178.
9. MacFarlane, D. R.; Meakin, P.; Sun, J.; Amini, N.. Pyrrolidinium Imides: A New Family of Molten Salts and Conductive Plastic Crystal Phases. *J. Phys. Chem. B* **1999**, *103*, 4164 –4170.
10. Welton, T., Room-Temperature Ionic Liquids. Solvents for Synthesis and Catalysis. *Chem. Rev.* **1999**, *99*, 2071 –2083.
11. Appetecchi, G. B.; Kim, G.T.; Montanina, M.; Carewska, M.; Marcilla, R.; Mecerreyes, D.; De Meatza, I. Ternary Polymer Electrolytes Containing Pyrrolidinium-Based Polymeric Ionic Liquids for Lithium Batteries. *J. Power Sources* **2010**, *195*, 3668-3675.
12. Lux, S. F.; Schmuck, M.; Jeong, S.; Passerini, S.; Winter, M.; Balducci, A. Li-ion Anodes in Air-Stable and Hydrophobic Ionic Liquid - Based Electrolyte for Safer and Greener Batteries. *Int. J. Energy Res.* **2010**, *34*, 97-106.

13. Kim, G. T.; Jeong, S. S.; Xue, M. Z.; Balducci, A.; Winter, M.; Passerini, S.; Alessandrini, F.; Appetecchi, G. B. Development of Ionic Liquid-Based Lithium Battery Prototypes. *J. Power Sources* **2012**, *199*, 239-246.

14. Barrosse-Antle, L. E.; Bond, A. M.; Compton, R. G.; O'Mahony, A. M.; Rogers, E. I.; Silvester. D. S. Voltammetry in Room Temperature Ionic Liquids: Comparisons and Contrasts with Conventional Electrochemical Solvents. *Chem. Asian J.* **2010**, *5*, 202 – 230.

15. Kim, H.; Ding, Y.; Kohl, P. A. LiSICON–Ionic Liquid Electrolyte for Lithium Ion Battery. J. *Power Sources* **2012**, *198*, 281– 286.

16. Appetecchi, G. B.; Montanino, M.; Passerini, S. Ionic Liquid-based Electrolytes for High-Energy Lithium Batteries in Ionic Liquids Science and Applications. ACS Symposium Series 1117, A. E. Visser, N. J. Bridges, R. D. Rogers editors, Oxford University Press, Inc., American Chemical Society, Washington, DC, USA (2013).

17. Liu, L.; Park, J.; Lin, X.; Sastry, A. M.; Lu, W. A Thermal-electrochemical Model that Gives Spatial-dependent Growth of Solid Electrolyte Interphase in a Li-ion Battery. *J. Power Sources* **2014**, *268*, 482-490.

18. Guan, P.; Liu, L.; Lin, X. Simulation and Experiment on Solid Electrolyte Interphase (SEI) Morphology Evolution and Lithium-Ion Diffusion. *J. Electrochem. Soc.* **2015**, *162*, A1798-A1808.

19. Brousselya, M.; Herreyreb, S.; Biensan, P.; Kasztejnac, P.; Nechevc, K.; Staniewic, R. J. Aging Mechanism in Li Ion Cells and Calendar Life Predictions. *J. Power Sources* **2001**, *97-98*, 13-21.

20. Yan, J.; Xia, B.-J.; Sub, Y.-C.; Zhou, X.-Z.; Zhang, J.; Zhang, X.-G. Phenomenologically Modeling the Formation and Evolution of the Solid Electrolyte Interface on the Graphite Electrode for Lithium-ion Batteries. *Electrochim. Acta* **2008**, *53*, 7069–7078.

21. Wang, A.; Kadam, S.; Li, H.; Shi, S.; Qi, Y. Review on Modeling of the Anode Solid Electrolyte Interphase (SEI) for Lithium-ion Batteries. *NPJ Comput. Mat.* **2018**, *4*, 15.

22. Takenaka, N.; Suzuki, Y.; Sakai, H.; Nagaoka, M. On Electrolyte-Dependent Formation of Solid Electrolyte Interphase Film in Lithium-Ion Batteries: Strong Sensitivity to Small Structural Difference of Electrolyte Molecules. *J. Phys. Chem. C* **2014**, *118*, 10874−10882.

23. Zheng, J.; Gu, M.; Chen, H.; Meduri, P.; Engelhard, M. H.; Zhang, J.-G.; Liu, J.; Xiao, J. Ionic Liquid-enhanced Solid State Electrolyte Interface (SEI) for Lithium–sulfur Batteries. *J. Mater. Chem. A* **2013**, *1*, 8464–8470.

24. Grande, L.; Paillard, E.; Kim, G.-T.; Monaco, S.; Passerini, S. Ionic Liquid Electrolytes for Li-air Batteries: Lithium Metal Cycling. *Int. J. Mol. Sci.* **2014**, *15*, 8122-8137.

25. Bhattacharyya, R.; Key, B.; Chen, H.; Best, A. S.; Hollenkamp, A. F.; Grey, C. P. In Situ NMR Observation of the Formation of Metallic Lithium Microstructures in Lithium Batteries. *Nat. Mater.* **2010**, *9*, 504−510.

26. Lvovich, V.; Wu, J.; Bennett, W.; Demattia, B.; Miller, T. Applications of AC Impedance Spectroscopy as Characterization and Diagnostic Tool in Li-Metal Battery Cells. *ECS Trans.* **2014**, *58*, 1−14.

27. Yildirim, H.; Haskins, J. B.; Bauschlicher, C. W. Jr.; Lawson, J. W. Decomposition of Ionic Liquids at Lithium Interfaces. 1. Ab Initio Molecular Dynamics Simulations. *J. Phys. Chem. C* **2017**, *121*, 28214−28234.

28. Haskins, J. B**.;** Yildirim, H.; Bauschlicher, C. W. Jr.; Lawson, J. W. Decomposition of Ionic Liquids at Lithium Interfaces. 1. Gas Phase Computations. *J. Phys. Chem. C **2017***, *121*, 28235−28248.

29. Strmcnik, D.; Castelli, I. E.; Connell, J. G.; Haering, D.; Zorko1, M.; Martins, P.; Lopes, P. P.; Genorio, B.; Østergaard, T.; Gasteiger, H.A.; Maglia, F.; Antonopoulos, B. K.; Stamenkovic, V. R.; Rossmeisl, J.; Markovic, N. M. Electrocatalytic Transformation of HF Impurity to H2 and LiF in Lithium-Ion Batteries. *Nat. Catal.* **2018**, *1*, 255–262.

30. Xiong, S.; Xie, K.; Blomberg, E.; Jacobsson, P.; Matic, A. Analysis of the Solid Electrolyte Interphase Formed with an Ionic Liquid Electrolyte for Lithium-Sulfur Batteries. *J. Power Sources* **2014**, *252*, 150-155.

31. Howlett, P. C.; MacFarlane, D. R.; Hollenkamp. A. F. High Lithium Metal Cycling Efficiency in a Room-Temperature Ionic Liquid. *Electrochem. Solid State Lett.* **2004**, *7*, A97-A101.

32. Chiang, H.-H.; Lu, J.-M.; Kuo, C.-L. First-principles Study of the Structural and Dynamic Properties of the Liquid and Amorphous Li–Si Alloys. *J. Chem. Phys.* **2016**, *144*, 034502.

33. Doh, C.-H.; Oh, M.-W.; Han, B.-C. Lithium Alloying Potentials of Silicon Anode of Lithium Secondary Batteries. *Asian J. Chem.* **2013**, *10*, 5739-5743.

34. Barrett, C.S. X-ray Study of the Alkali Metals at low temperatures. *Acta Cryst.* **1956**, 9, 671-677.

35. Lin, S.-T.; Maiti, P. K.; Goddard III, W. A. Two-Phase Thermodynamic Model for Efficient and Accurate Absolute Entropy of Water from Molecular Dynamics Simulations. *J. Phys. Chem. B* **2010**, *114*, 8191-8198.

36. Pascal, T. A.; Lin, S.-T.; Goddard III, W. A. Thermodynamics of Liquids: Standard Molar Entropies and Heat Capacities of Common Solvents from 2PT Molecular Dynamics. *Phys. Chem. Chem. Phys*. **2011**, *13*, 169-181.

37. Pascal, T. A.; Goddard, W. A.; Jung, T. Entropy and the Driving Force for the Filling of Carbon Nanotubes with Water. *Proc. Nat. Acad. Sci. USA* **2011**, *108*, 11794-11798.

38. Pascal, T. A.; He, Y.; Jiang, S.; Goddard III, W. A. Thermodynamics of Water Stabilization of Carboxybetaine Hydrogels from Molecular Dynamics Simulations. *J. Phys. Chem. Lett.* **2011**, *2*, 1757-1760.

39. Pascal, T. A.; Goddard, W. A.; Maiti, P. K.; Vaidehi, N. Role of Specific Cations and Water Entropy on the Stability of Branched DNA Motif Structures. *J. Phys. Chem. B* **2012**, *116*, 12159-12167.

40. Huber, K.-P. Molecular Spectra and Molecular Structure: IV. Constants of Diatomic Molecules. (Springer Science & Business Media, 2013).

41. van Duin, A. C. T.; Dasgupta, S.; Lorant, F.; Goddard, W. A. ReaxFF: A Reactive Force Field for Hydrocarbons. *J. Phys. Chem. A* **2001**, *105*, 9396–9409.

42. Kresse, G.; Furthmuller, J. Efficiency of Ab-Initio Total Energy Calculations for Metals and Semiconductors Using a Plane-Wave Basis Set. *Comput. Mater. Sci.* **1996**, *6*, 15 – 50.

43. Kresse, G.; Furthmuller, J. Efficient Iterative Schemes for Ab Initio Total-Energy Calculations Using a Plane-Wave Basis Set. *Phys. Rev. B* **1996**, *54*, 11169 - 11186.

44. Kresse, G.; Joubert, D. From Ultrasoft Pseudopotentials to the Projector Augmented-Wave Method. *Phys. Rev. B* **1999**, *54*, 1758 - 1775.

45. Perdew, J.; Burke, K.; Ernzerhof, M. Generalized Gradient Approximation Made Simple. *Phys. Rev. Lett.* **1996**, *77*, 3865 - 3868.

46. Grimme, S.; Antony, J.; Ehrlich, S.; Krieg, H. A Consistent and Accurate Ab Initio Parametrization of Density Functional Dispersion Correction (DFT-D) for the 94 Elements H-Pu. *Chem. Phys.* **2010**, *132*, 154104.

47. Grimme, S.; Ehrlich, S.; Goerigk, L. Effect of the Damping Function in Dispersion Corrected Density Functional Theory. *J. Comp. Chem.* **2011**, *32*, 1456.

48. Aykol, M.; Kim, S.; van der Waals, C. W. Interactions in Layered Lithium Cobalt Oxides. *J. Phys. Chem. C* **2015**, *119*, 33, 19053-19058.

49. Kravchyk, K. V.; Bhauriyal, P.; Piveteau, L.; Guntlin, C. P.; Pathak, B.; Kovalenko, M. V. High-energy-density Dual-ion battery for Stationary Storage of Electricity Using Concentrated Potassium Fluorosulfonylimide. *Nat. Commun.* **2018**, *9*, 4469.

50. Kabiraj, A.; Mahapatra, S. High-throughput First-principles-calculations Based Estimation of Lithium Ion Storage in Monolayer Rhenium Disulfide. *Commun. Chem.* **2018**, *1*, 81.

51. Kostenetskiy, P.; Semenikhina, P. SUSU Supercomputer Resources for Industry and Fundamental Science (2018) Proceedings - 2018 Global Smart Industry Conference, GloSIC, 8570068.